



*Citation for published version:*

Almond, DP, Angioni, SL & Pickering, SG 2017, 'Long pulse excitation thermographic non-destructive evaluation', *NDT and E International*, vol. 87, pp. 7-14. <https://doi.org/10.1016/j.ndteint.2017.01.003>

*DOI:*

[10.1016/j.ndteint.2017.01.003](https://doi.org/10.1016/j.ndteint.2017.01.003)

*Publication date:*

2017

*Document Version*

Peer reviewed version

[Link to publication](#)

*Publisher Rights*

CC BY-NC-ND

**University of Bath**

**Alternative formats**

If you require this document in an alternative format, please contact:  
[openaccess@bath.ac.uk](mailto:openaccess@bath.ac.uk)

**General rights**

Copyright and moral rights for the publications made accessible in the public portal are retained by the authors and/or other copyright owners and it is a condition of accessing publications that users recognise and abide by the legal requirements associated with these rights.

**Take down policy**

If you believe that this document breaches copyright please contact us providing details, and we will remove access to the work immediately and investigate your claim.

## **Long pulse excitation thermographic non-destructive evaluation.**

Darryl P Almond, Stefano L Angioni and Simon G Pickering.

RCNDE, Department of Mechanical Engineering, University of Bath, Bath, BA2 7AY, UK.

Corresponding author e-mail address: [mssdpa@bath.ac.uk](mailto:mssdpa@bath.ac.uk) (D.P.Almond)

Keywords: thermography, long pulse, sensitivity.

### **Abstract**

A comprehensive analysis of the defect detection performance of long pulse excitation thermographic NDE is presented. An analytical procedure for predicting the thermal image contrasts of defects of specified size and depth is developed and validated by extensive experimental studies of test pieces having a wide range of thermal properties. Results obtained using long pulse (~5 sec.) excitation are compared with those obtained using traditional flash excitation. The conditions necessary for the success of the long pulse method are explained and illustrated by both modelling and experimental results. Practical advantages of long pulse excitation are discussed.

### **1, Introduction**

The most widely used form of active thermographic non-destructive evaluation (NDE) employs the same short (~2 ms) pulse or flash excitation introduced by the pioneers [1, 2] of the technique in the early 1980s. Their work followed earlier studies of Green [3] in 1965 and Carlomagno and Berardi [4] in 1976. The history of the thermographic NDT techniques can be found in the recent review by Vavilov and Burleigh [5]. Following the flash heating of a component under inspection by a number of high optical intensity flash lamps, the subsequent transient in surface temperature is monitored with an infrared camera. The technique is particularly suitable for the detection and imaging of near surface, in-plane, defects such as delaminations in composite materials or adhesion defects between coatings and their substrates. These defects block the flow of heat from a flash heated surface, causing a reduction in the cooling rate of the surface above the defects that is

revealed as an area of thermal contrast in the thermal images of the surface collected by an infrared camera. Whilst the technique has the attractions of simplicity of implementation and of providing a rapid inspection of large areas, its take-up has been restricted, in part, by the high cost of the equipment employed. In recent years, the costs of infrared cameras have reduced enormously and they have become increasingly common in the workplace. However, the high optical intensity flash lamp systems that are typically employed by users of the technique remain pieces of expensive and specialist equipment.

A number of alternative thermal stimulation schemes have been developed. Modulated heating is used for lock-in thermography [6] and more complex modulations are used for frequency modulated thermography [7]. In these cases inexpensive lamps can be used but they have to be driven by power amplifiers and specialised processing of the thermal images is required. The simplest means of applying a thermal stimulation to a surface is to expose it to a high intensity heat source for a few seconds. Many workers in the field are aware that this long pulse excitation technique can be effective for some favourable applications. The technique has a long history [8-10] and it is offered by some commercial companies [11, 12]. However, there appears to have been little detailed study of the capabilities of thermographic NDE employing this “long pulse” mode of thermal stimulation. Here we must distinguish between long pulse thermography and step heating thermography that has received more attention [13-15]. In long pulsed thermography, heating is applied for a selected period of time, eg 5 sec., and then thermal images are collected as the test piece cools down. In step heating thermography, thermal images are collected whilst the test piece is heated up. The technical advantages of long pulse over step heating thermography will be explained later.

In this paper, an analytical analysis of long pulse excitation thermographic NDE is presented. This analytical analysis elucidates the role that the thermophysical properties have in determining the defect detection capabilities of the technique. The results of an experimental study are also presented and compared with analytical predictions. A comparison is also made with the performance of the traditional flash excitation technique. It is found, in some cases, that the long pulse technique

performs very favourably compared with the flash excitation technique and that it has practical and economic advantages over the traditional method.

## 2, Analytical Analysis.

In a recent analytical analysis [16] of the defect detection performance of flash excitation thermographic NDE, the thermal contrast,  $Tc(t)$ , at the surface over the centre of a circular, in-plane, defect of diameter  $D$  at a depth  $d$  was shown to be:

$$Tc(t) = \frac{2J_0}{\sqrt{\pi\rho ckt}} \left[ \sum_{n=1}^{\infty} e^{-\frac{(nd)^2}{\alpha t}} \right] \left( 1 - e^{-\frac{(D/2)^2}{4\alpha t}} \right) \quad (1)$$

in which  $J_0$  is the thermal energy density ( $\text{Jm}^{-2}$ ) created at the surface by absorption of the optical flash excitation,  $\rho$ ,  $c$ ,  $k$  and  $\alpha$  are the density, heat capacity, thermal conductivity and thermal diffusivity of the test piece material and  $t$  is time after impulse excitation. The term in the square brackets arises from the contrast produced by a layer of thickness  $d$  [17]. The term in the curved brackets is a decay term that accounts for the lateral diffusion of heat trapped between the defect and the surface to the cool edges of the defect, a distance  $D/2$  from the defect centre. It is assumed that the defect is perfectly insulating and blocks all heat flow across it. In practice, this corresponds to a wide open delamination or an artificial defect in the form of a back-drilled flat bottomed hole. A refinement of the model, in which heat transfer is allowed across defects of narrower openings, will be the subject of a future publication.

The thermal impulse response predicted by eqn. 1 was shown [16] to accurately account for the principle features of the peak in defect image contrast that follows flash excitation. An example of such a peak is shown in figure 1. These results are for a 5mm diameter circular in-plane defect 1mm beneath the surface in a mild steel sample subjected to a heating impulse,  $J_0$ , of  $10 \text{ kJ m}^{-2}$ . Finite difference numerical modelling results are also shown in the figure for comparison. It is evident that the analytical expression gives a remarkably good approximation of the early part of the contrast-time curve, the peak contrast and the time at which contrast peaks. At times after the peak, the analytical

expression over estimates thermal contrast, indicating the long time thermal decay of contrast to be more complex than the simple diffusion of heat to the defect edge.

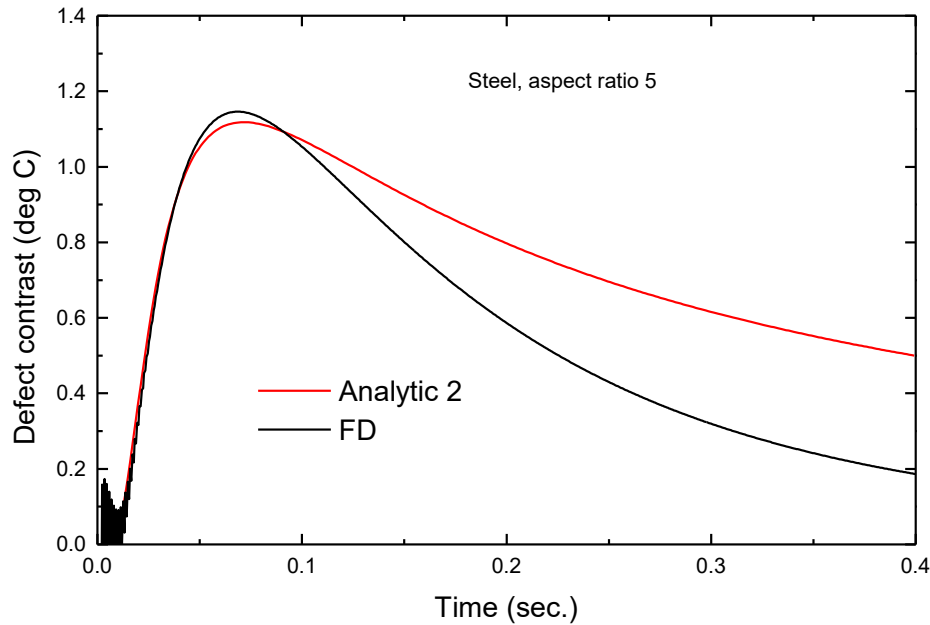


Figure 1. Thermal contrast vs. elapsed time for a 5mm diameter defect 1mm beneath the surface of a mild steel sample calculated by finite difference modelling (FD) and the analytical model, eqn.1, (Analytic 2). Pulse intensity  $10 \text{ kJ m}^{-2}$ .

In the above basic analytical model, the defect is assumed to be in a solid whose thickness is very much greater than the defect depth. In such a solid the thermal decay of the surface above sound material can be assumed to be unaffected by thickness. For thinner plates, this thermal decay is affected and its alteration is important because the temperature over sound regions surrounding a defect provides the reference with respect to which defect image contrast is observed/measured. To deal with this, the contrast is re-defined as being the difference in temperature at the surface over the defect compared with the temperature over a sound region of a plate of specified thickness  $L$ . The revised expression becomes:

$$Tc(t) = \frac{2J_0}{\sqrt{\pi\rho ck t}} \left[ \sum_{n=1}^{\infty} e^{-\frac{(nd)^2}{\alpha t}} - \sum_{n=1}^{\infty} e^{-\frac{(nL)^2}{\alpha t}} \right] \left( 1 - e^{-\frac{(D/2)^2}{4\alpha t}} \right) \quad (2)$$

The long pulse excitation response can be obtained by representing it as being a sequence of impulse responses. The defect image thermal contrast,  $Tc(t)$ , may be obtained by integration of the impulse response function:

$$Tc(t) = \int_{\tau=0}^{t_p} \frac{2W}{\sqrt{\pi\rho ck(t+\tau)}} \left[ \sum_{n=1}^{\infty} e^{-\frac{(nd)^2}{\alpha(t+\tau)}} - \sum_{n=1}^{\infty} e^{-\frac{(nL)^2}{\alpha(t+\tau)}} \right] \left( 1 - e^{-\frac{(D/2)^2}{4\alpha(t+\tau)}} \right) d\tau \quad (3)$$

In equation 3,  $W$  is power density or heat flux ( $Wm^{-2}$ ) created at the surface by the absorption of optical energy from lamps applied for a duration of  $t_p$ . The total long pulse thermal excitation energy of  $Wt_p$  is formed by a sequence of impulses  $Wd\tau$  applied for the pulse duration time  $t_p$  and the image contrast of each of these is added to compute the total contrast generated at a time  $t$  after the end of the heating period. For the long pulse technique to be effective, the majority of the energy applied by the pulse needs to contribute to the contrast observed at the end of pulse heating. The time scale for the development and decay of defect image contrast, such as shown in figure 1, is highly dependent on the thermophysical properties of the host material. In fig.1, the contrast peaks at  $\sim 0.07$  seconds after the impulse and has decayed significantly by 0.4 seconds. A negligible contrast would remain after a typical long pulse excitation time,  $t_p$ , of 5 seconds. Consequently, it may be concluded that the early elements,  $Wd\tau$ , will make little contribution to final image contrast in a case such as that shown in fig.1 where contrast peak time is far shorter than the long pulse excitation time  $t_p$ . In such cases, the final image contrast arises only from elements towards the end of the heating pulse and the effective heating pulse energy is reduced from  $Wt_p$  to  $Wt_{eff}$ . where  $t_{eff} \ll t_p$ .

Contrast peak times vary with the inverse of thermal diffusivity. The thermophysical properties and contrast peak times, calculated using eqn. 1 for the same 5mm diameter defect 1 mm

beneath the surface, in four common engineering materials: aluminium alloy, mild steel, stainless steel and carbon fibre reinforced plastic (CFRP), are shown in Table 1.

Material	Thermal Conductivity k Wm <sup>-1</sup> K <sup>-1</sup>	Specific Heat c Jkg <sup>-1</sup> K <sup>-1</sup>	Density ρ Kg m <sup>-3</sup>	Thermal Diffusivity α 10 <sup>-6</sup> ms <sup>-2</sup>	Flash Peak Contrast Time Eqn.1 (s)	Long Pulse Peak Contrast Eqn. 3 (deg. C)	Long Pulse Peak Contrast Finite Diff. (deg. C)
Al. alloy	177	875	2770	73	0.017	0.034	0.016
Mild steel	64	434	7830	18.8	0.07	0.08	0.04
Stainless steel	13.4	468	8230	3.47	0.36	0.21	0.16
CFRP	1	1200	1700	0.5	1.8	0.49	0.48

**Table 1**, Thermophysical properties, flash excitation peak contrast times and long pulse peak contrasts of 5mm diameter 1mm deep defects in materials indicated. 5 second heating of 1kWm<sup>-2</sup>.

Finite difference simulations of the thermal contrasts produced over the centres of 5mm diameter defects 1mm below the surface in aluminium alloy, mild steel, stainless steel and CFRP samples exposed to a heat flux of 1kWm<sup>-2</sup> for 5 seconds are shown in figure 2. Little thermal contrast occurs for the high thermal conductivity/diffusivity aluminium alloy and mild steel samples whilst there is a useable contrast for the stainless steel sample and a strong contrast for the low thermal conductivity/diffusivity CFRP sample. The aluminium alloy and mild steel simulations show a rapid saturation of thermal contrast whilst the stainless steel and CFRP results show a steady accumulation of contrast throughout the heating period. These results are consistent with the above interpretation as peak contrast times, Table 1, for aluminium alloy and mild steel are far shorter than for stainless steel and CFRP. The magnitudes of peak contrasts of the same defects in 6mm thick sheet material calculated by the analytical expression, eqn.3, are compared with the independent finite difference results, fig.2, in the table. It is evident that the analytical expression, whilst showing the same trend, overestimates long pulse contrast by increasing proportions as test piece thermal diffusivity increases. This can be traced to the difference in the flash excitation contrast peaks predicted by the two methods shown in fig. 1. The excess in contrast obtained by the analytical model at long times contribute strongly to the integral in eqn. 3 where peak contrast times are very short compared to long pulse

duration of 5 seconds. Where they are not, eg CFRP, little of the excess contributes and agreement between the two methods is good.

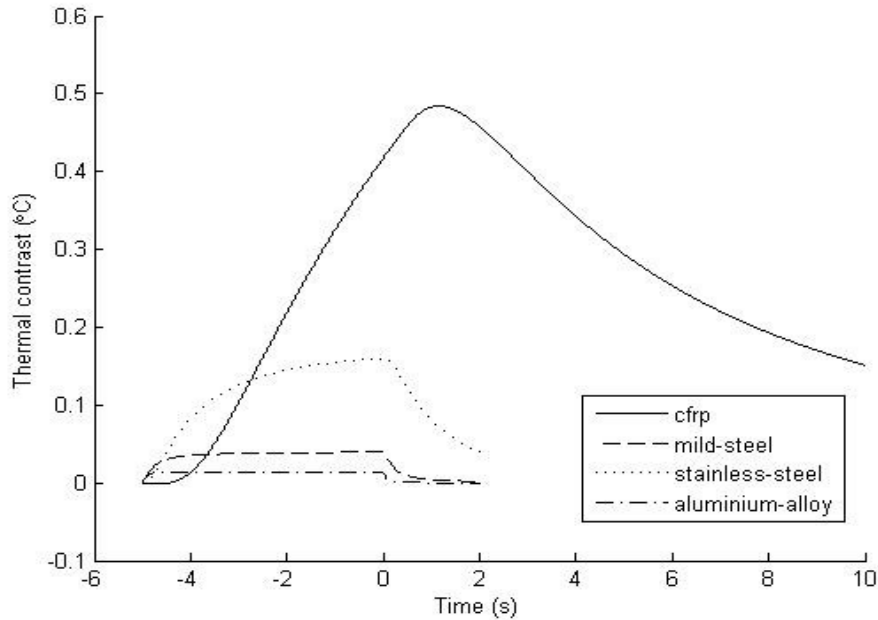
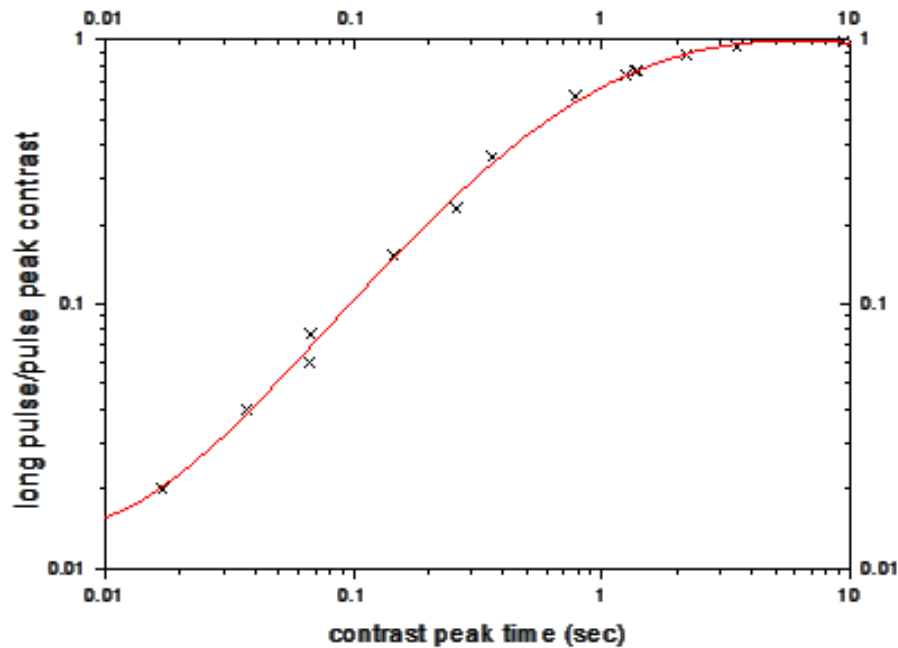


Figure 2, Finite difference simulation of long pulse thermal contrast vs. time for 5mm diameter 1mm deep defects in materials indicated. 5 second heating of  $1\text{kWm}^{-2}$ .

The relationship between long pulse thermal contrast and flash excitation peak contrast time is shown in figure 3. This figure shows finite difference calculations of the ratio of long pulse contrast to flash excitation contrast for defects, obtained using the same excitation energy ie setting  $Wt_p = J_0$ , plotted against the time of the peak in contrast for flash excitation. This ratio can be seen to rise monotonically with peak contrast time where this time is much shorter than the pulse heating time of 5 seconds. For the longer values of peak contrast time the ratio of long pulse contrast to flash excitation peak contrast approaches one. This is an important result because it indicates the long pulse technique to have almost the same defect detection capability as the flash excitation technique for combinations of thermophysical properties and defect geometries that result in long peak contrast times. Moreover, figure 3 can be used to assess long pulse contrast for a particular defect in a specified material because flash excitation peak contrast times and contrasts for the same defect can be estimated rapidly from equation 1 or 2. Hence figure 3 provides a simple means of assessing the



prospect of using the long pulse technique as an alternative to the flash excitation technique. As numerical modelling was used for the calculations, results obtained from the relationship shown in figure 3 overcome the overestimations of long pulse contrast found using the analytical model, eqn.3.



**Figure 3.** Ratio of long pulse to flash peak contrast shown as a function of flash contrast peak time.

### 3, Experimental Methods

The test pieces used were square 6 mm thick plates of side length 200 mm made from aluminium alloy, mild steel and stainless steel and a 10 mm thick square CFRP composite plate of side length 300mm. Flat-bottomed back-drilled holes (FBH) of varying diameters and depths were drilled in the samples to represent in-plane defects. The aluminium alloy, mild steel and stainless steel samples contained FBH defects with diameters of 10, 14 or 15 and 20mm drilled to distances from the test piece surfaces in the range 0.5 to 4mm. The CFRP plate contained FBH defects of 10, 16 and 20mm diameter at depths from 0.5 to 4.25 mm. All of the samples were painted using matt black acrylic spray paint to maximise optical energy absorption and emissivity.

Long pulse heating was provided by a pair of 1kW quartz halogen lamps positioned as illustrated in figure 4 to produce a fairly uniform illumination of the test pieces. Drop plate shutters were used to shield the test piece from the lamps' residual infrared emissions when they were switched off after a heating period of ~5 s. These shutters were elastically accelerated and closed within an IR camera frame time (1/60 s). The shutters improved the defect image contrasts obtained from the metallic test pieces significantly. For the metals, these contrasts, see fig.2, only persist a short time after heating, requiring thermal imaging when the residual infrared emissions of the lamps are at their highest.

The test pieces were also imaged by conventional flash excitation thermography. The two quartz halogen lamps were replaced by a pair of 3kJ Hensel [18] Xenon flash lamps, positioned in the same way as shown in figure 4. The shutters were not used with the flash lamps, which matches the general practice in the use of these lamps. This may have resulted in some reduction of image contrast caused by the reflection into the IR camera of IR radiation from flash lamp parts heated during the flash emission process. This afterglow effect decays with time as the parts cool down but may be significant for about a second after the flash, making it a potential problem in the imaging of defects in metallic parts. The magnitude of the effect depends on the lamp construction and characteristics, the geometry of the experimental setup and the IR reflectivity of the test piece surface. It can be reduced by the use an IR absorbing filter such as a sheet of polymethyl methacrylate (PMMA). This was not done here as adequate images of the test pieces were obtained for the required qualitative comparison with the long pulse excitation images, detailed in Section 4 below.

The camera, an Indigo Merlin mid wave IR camera, has a maximum frame rate of 60Hz and an NEdT (noise level) of less than 25mK (and typically <18mK).

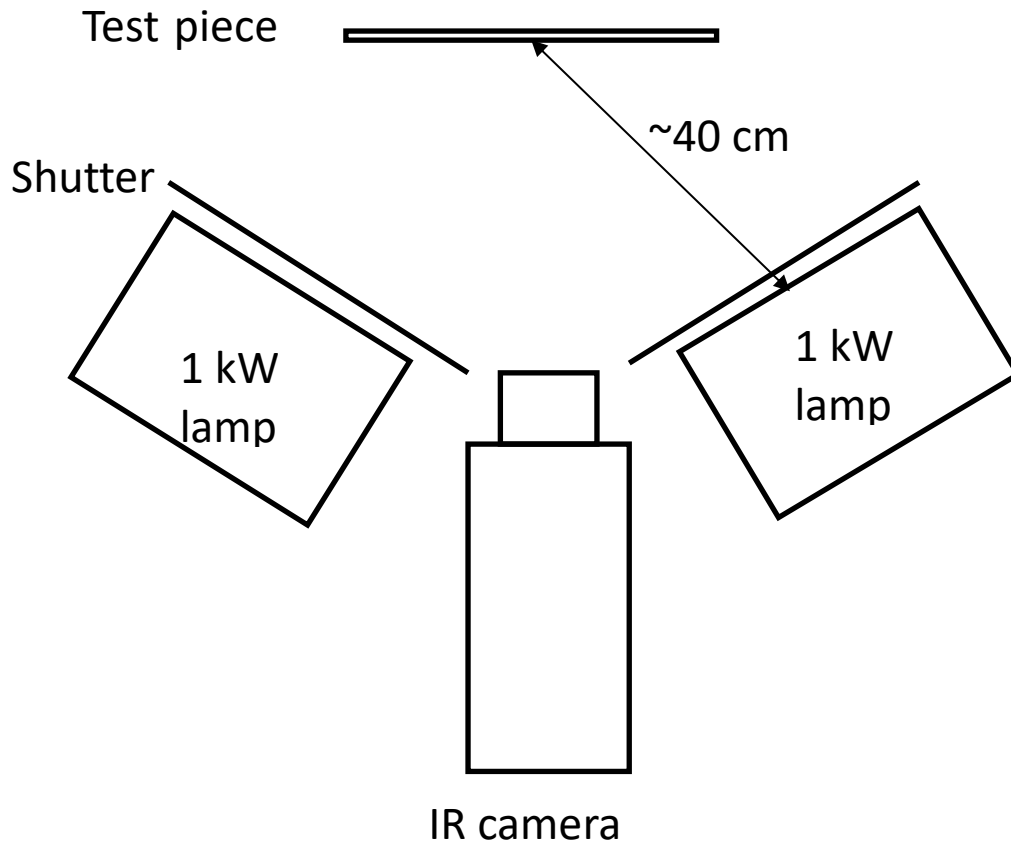
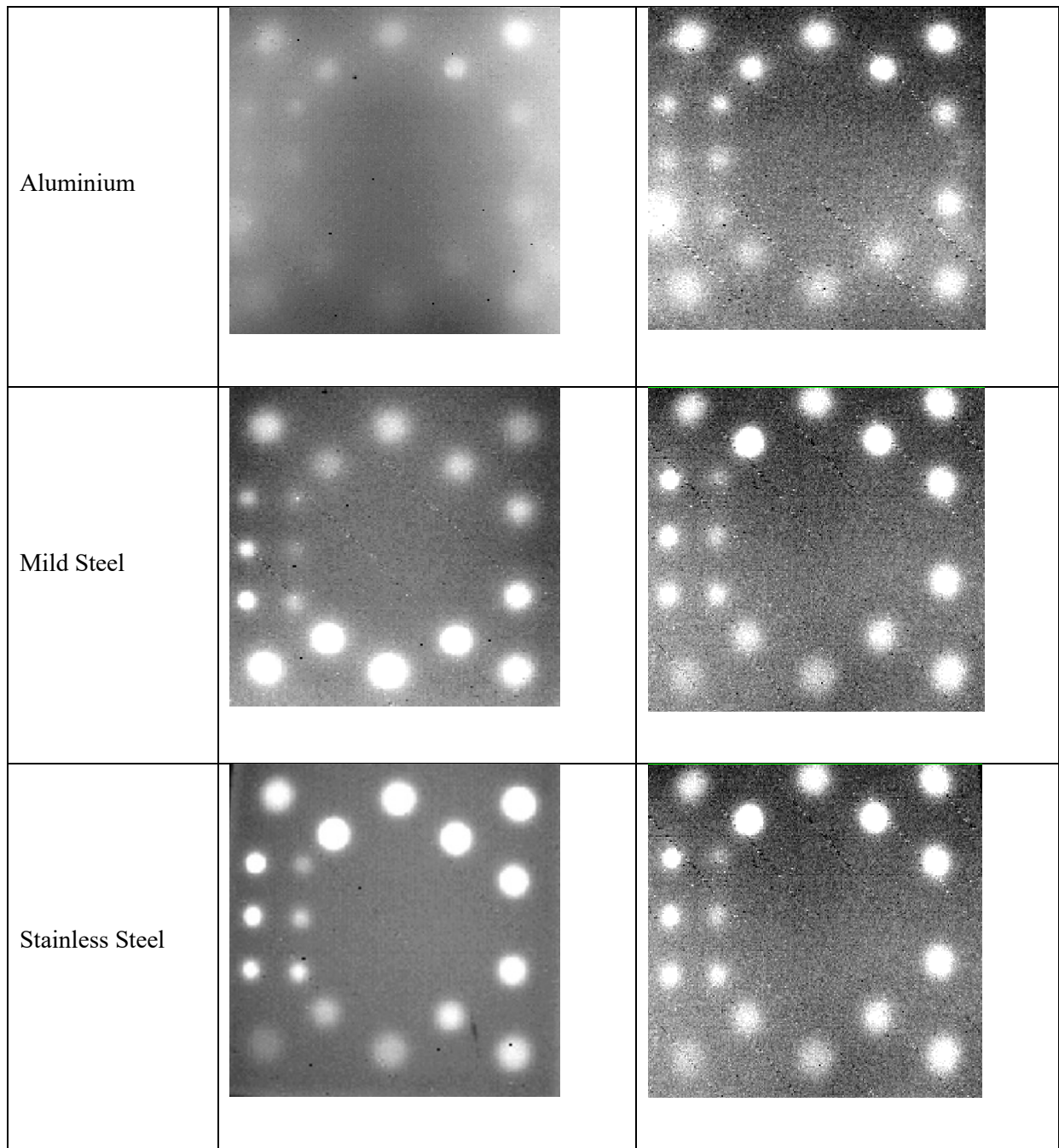


**Figure 4.** Schematic diagram of the long pulse excitation thermographic NDE system.

#### 4, Experimental Results.

Long pulse and flash excitation images of the metallic test pieces are shown in figure 5.

	Long pulse	Flash
--	------------	-------

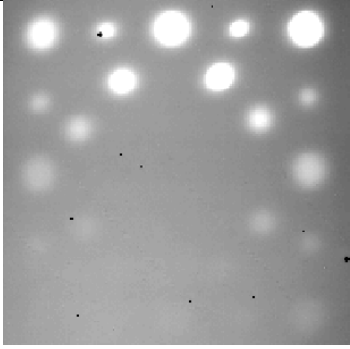
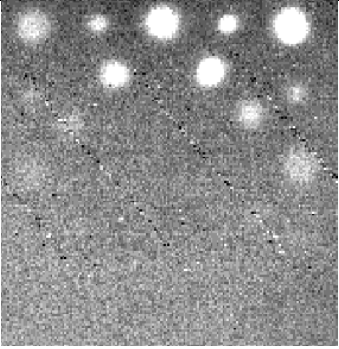
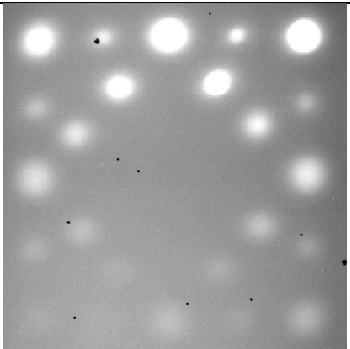
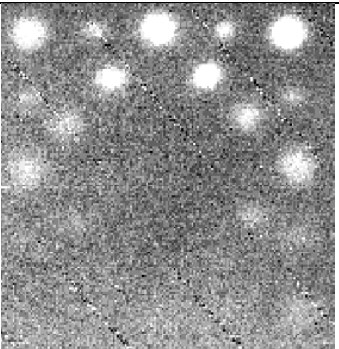


**Figure 5.** Long pulse and flash excitation images of the aluminium alloy, mild steel and stainless steel test pieces.

The long pulse images shown were the first images recorded at the end of the heating after the shutters had closed. The flash excitation images shown were selected from the image sequence recorded after flash excitation as being the images showing the best overall pictures of the defects in the test pieces. As expected, the long pulse images of the defects in the aluminium alloy test piece

have the lowest contrasts whilst similar contrasts were achieved for all three test pieces using the flash excitation technique.

Long pulse and flash excitation images of the CFRP test pieces are shown in figure 6. For this test piece, images obtained at 5, 10, 15 and 20 seconds after heating are shown. This is necessary because the image contrasts of defects at different depths peak at times that are many seconds apart because of the low thermal diffusivity of CFRP. The deeper defects were concentrated in the lower part of the test piece and it can be seen that these only appear in the images recorded at the longer times after the termination of heating.

	Long Pulse	Flash
5 seconds		
10 seconds		

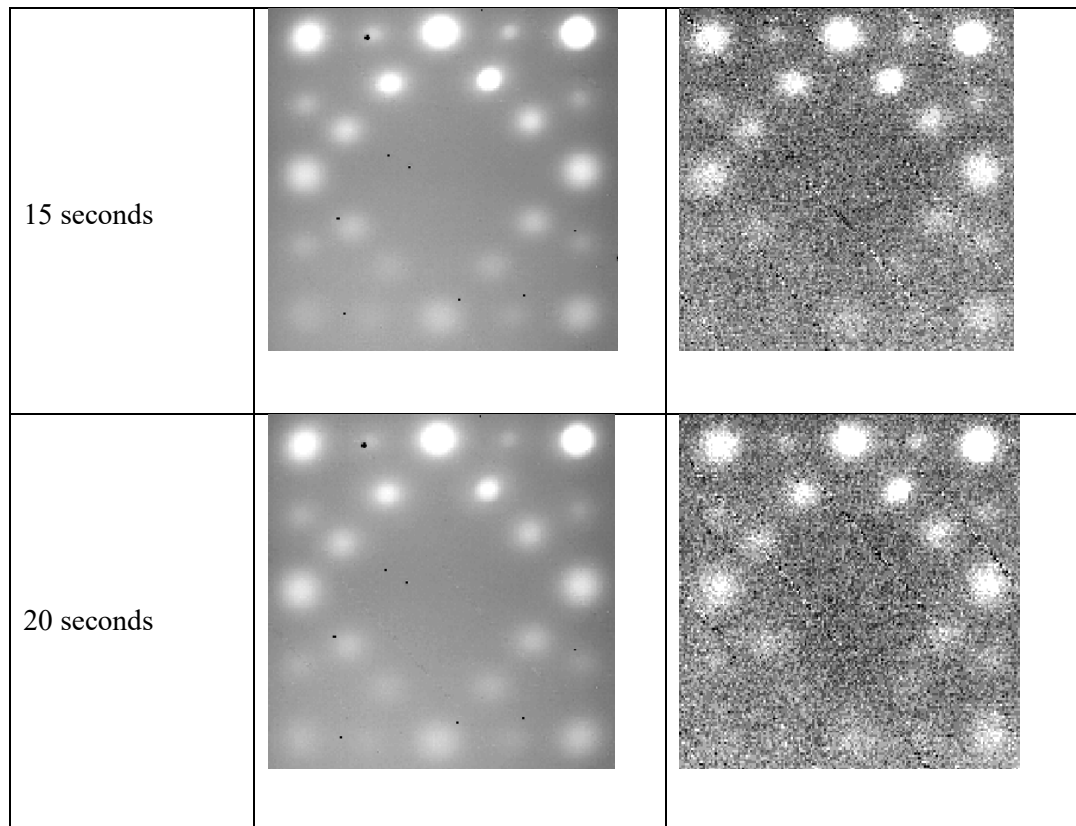


**Figure 6.** Long pulse and flash excitation images of the CFRP test piece obtained at 5, 10, 15 and 20 seconds after heating.

#### **4.1 Methods of analysis of long pulse excitation experimental results.**

The contrast of a defect image is defined as the difference between the temperature rise at the centre of a defect image and the background temperature rise at the same position in defect free material. The background temperature rise for each defect was estimated from the temperature rises in four square regions on the test pieces set just above and below and to the right and left of the defect, illustrated in figure 7a. The average value of the temperature rise in these four regions was used as an estimate of the temperature rise that would have occurred over the defect centre, in the absence of the defect. The temperature rise at the centre of a defect image was obtained from the average value of temperature rise in a smaller box (typically 3x3 mm), fig 7a, set about the centre of the defect image. The three metallic test pieces were imaged using a 60 Hz frame rate.

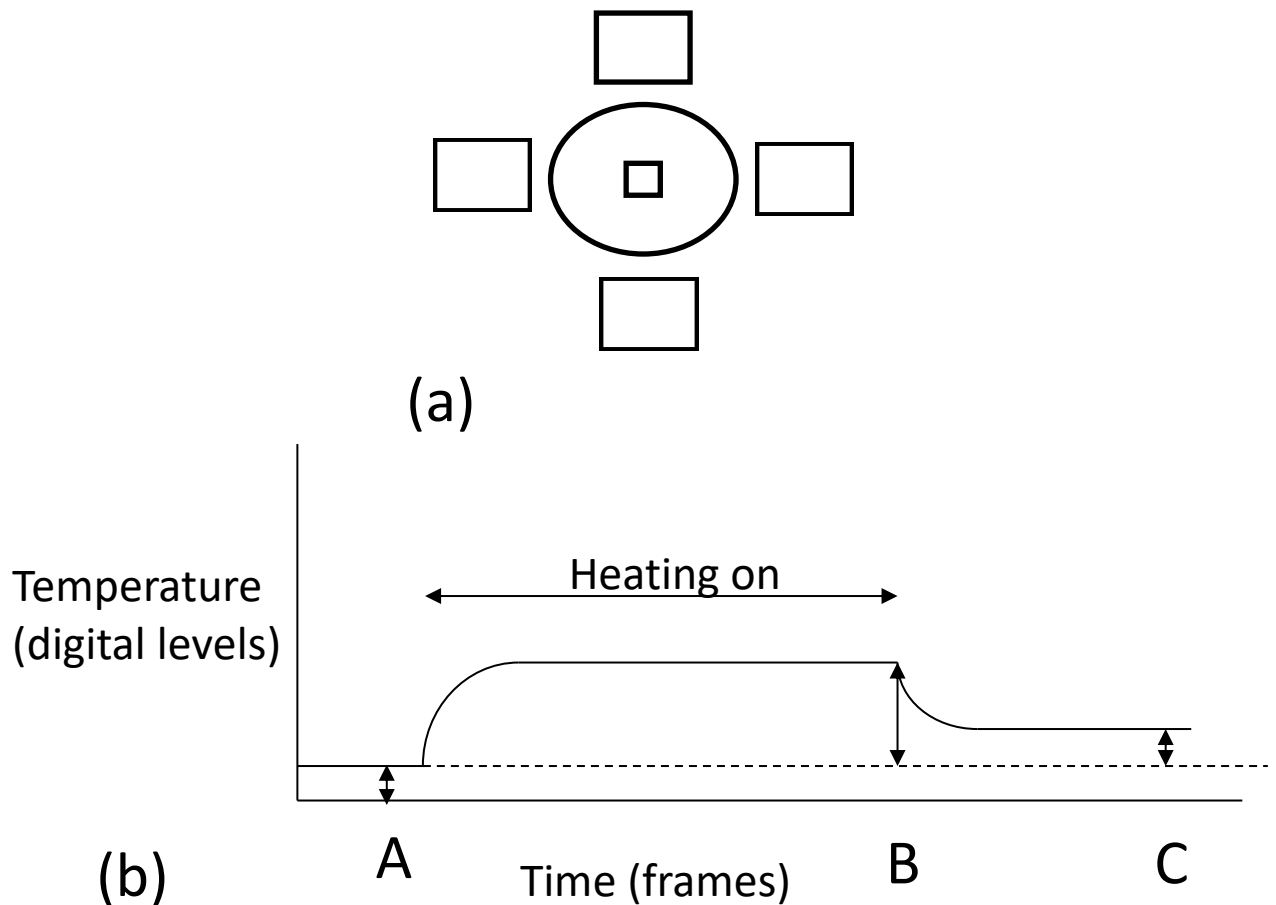


**Figure 7.** (a) Schematic diagram showing the locations of the four boxes of pixels around a defect image used to estimate background heating and the smaller box of pixels within image used to estimate image contrast. (b) Schematic timing diagram for a typical pixel showing the effect of heating and subsequent cooling on the recorded digital signal.

The measurement procedure was to record a sequence of 547 IR camera images (frames) covering the heating and subsequent cooling of a test piece. Figure 7b is a schematic diagram showing the digital signal change from frame to frame for a pixel of the recorded IR image. The IR camera pixel signals were 12 bit digitised and a calibration showed a change of 1100 digital levels to correspond to a temperature rise of  $1^{\circ}\text{C}$ . The recording was started before the heating lamps were switched on to provide a measure of the camera signal at each point across the test piece prior to heating, level A in fig 7b. The heating lamps were then switched on for  $\sim 5$  seconds, switched off and the shutters were released. The actual period of heating for each test was obtained by examination of the video record. The beginning of heating was shown by lamp reflection from an unpainted metallic

part in the field of view and the termination of heating was shown by the sharp elimination of this reflection on the closure of the shutters. The accuracy of this measurement was estimated to be about a frame period, ie 1/60 second. For the three metallic test pieces defect image contrasts were measured at the end of heating, on the closure of the shutters.

The CFRP test piece was imaged using a 15 Hz frame rate because thermal response rate of CFRP is far slower than that of the metals. A result of this is the peaking of thermal images of defects at a significant time, often many seconds, after the termination of long pulse heating, as shown in figure 2. Consequently, it was necessary measure the contrasts of the CFRP defect images in frames recorded at these times at which contrast peaked.

The timing diagram, fig 7b, shows the heating to cause a rise in temperature during heating followed by a cooling transient, at B, and a settling at a temperature, at C, above the initial test piece temperature, A. During heating a temperature gradient is maintained through the thickness of the test piece. When the heating ceases heat flows into the test piece and the surface cools, illustrated by the cooling transient at B. However, for a test piece of finite thickness the heat applied to the surface is trapped within the plate and causes the temperature of the plate to rise, to the level indicated at C. The magnitude of this temperature rise is simply  $Wt_p/(\rho cL)$ , since  $Wt_p$  is the thermal energy applied to the surface by the long pulse heating and  $(\rho cL)$  is the heat capacity per unit area of a plate of thickness  $L$ . An assumption is made that for short times after heating conditions are adiabatic, ie there is negligible heat loss from the plate by convection or radiation. This assumption is supported by the small temperature increase measured in the experiments of  $\sim 0.6$  °C and by the results of numerical modelling that show the inclusion of convective heat losses to have a negligible effect on results for the four test pieces examined. The simple relationship, above, between this temperature rise and  $W$  provides a valuable means of estimating the heat flux  $W$  produced by the lamps locally at any point across the test pieces. In this work, the magnitude of  $W$  over the centre of each defect was estimated from the average of the long-time temperature rises in the four boxes surrounding each defect. This value was used to compare measured contrasts with the contrast predicted for each defect by equation 3 and figure 3, setting  $J_0=Wt_p$ .



## 4.2 Analysis of experimental results.

The measurements of the contrasts of the defect images are shown in figure 8 plotted against their depths. The error bars shown are one standard deviation of the data in the small boxes of pixels used to estimate the contrast. This standard deviation was found to be consistently  $\sim 10\%$  of the measured contrast. Also shown in the figure are the values of contrast predicted for each defect by use of equation 3 and figure 3, as outlined in section 2. Each of these predictions made use of the local estimate of heat flux,  $W$ , explained above. This was found to vary from  $\sim 1900 \text{ Wm}^{-2}$  for the defects closest to the edges of the test pieces to  $\sim 2200 \text{ Wm}^{-2}$  for those towards the centres.

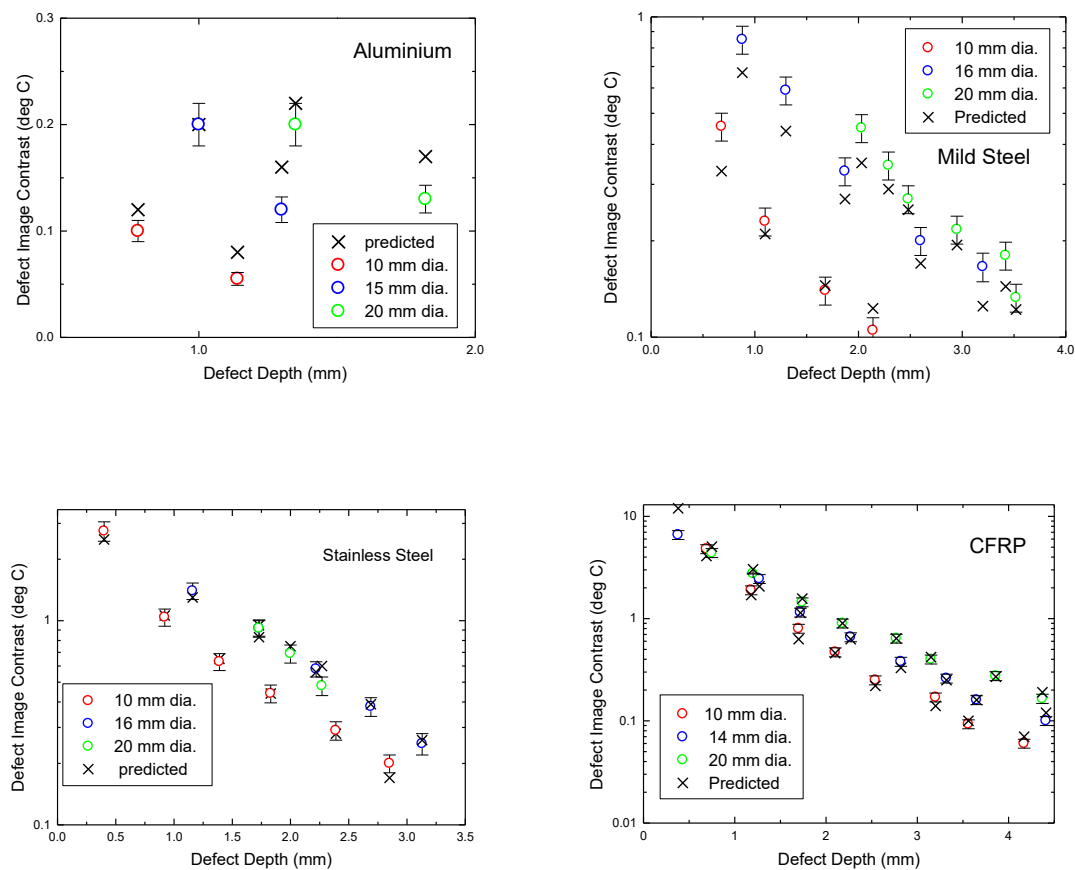


**Figure 8**, Measurements of the contrasts of the long pulse excitation images, shown in figures 5 and 6, of the defects compared with contrasts predicted by the analytical method outlined in section 2.

## 5, Discussion.

In this work the defect detection performance of thermographic NDE using long pulse excitation has been studied in four different commonly used engineering materials. The materials were also chosen because their thermal properties (thermal conductivity and diffusivity) spanned the very wide range covered by commonly used engineering materials. The four test pieces were furnished with similar collections of artificial defects to enable comparisons to be made of the effect of material properties on defect detection performance. The images of the test pieces, figs. 5 and 6, show both the effectiveness of the long pulse excitation technique for the detection of defects in low thermal conductivity/diffusivity materials and its ineffectiveness for the detection of similar defects in high thermal conductivity/diffusivity materials. By contrast, the traditional flash excitation method is equally effective at defect detection in both high and low thermal conductivity materials, as can be seen in the accompanying flash excitation images of the test pieces included in figs. 5 and 6. The flash excitation images are noisier and of lower contrast than the long pulse excitation images because the excitation energy,  $J_0$ , produced by the two 3 kJ xenon flash lamps was much lower than the excitation energy,  $Wt_p$ , produced by the two 1 kW quartz halogen illuminated for 5 seconds. In the tests,  $J_0$  was found to be  $\sim 3 \text{ kJm}^{-2}$  whilst the product  $Wt_p \sim 2 \text{ kWm}^{-2} \times 5 = \sim 10 \text{ kJm}^{-2}$ . The ease and advantages of achieving high excitation energies by long pulse excitation methods will be discussed later.

The analytical analysis of the long pulse excitation imaging process showed the magnitude of defect image contrast to depend on the thermal response rate of a material. The key parameter that characterises this response rate for the imaging of a specific defect in a particular material is the time at which the defect image peaks in contrast after the flash excitation of the material's surface. This time can be readily obtained from eqns.1 or 2 that model the temporal development of defect image contrast following flash excitation. It was found that contrast achieved by long pulse excitation was the simple function of this flash excitation peak contrast time shown in fig.3. Hence, the analytical analysis indicates eqns. 1 or 2 and fig.3 to provide a means of estimating long pulse excitation defect image contrast. This analysis has been tested comprehensively by measuring the contrasts of the

defect images shown in figs. 5 and 6 and comparing them with the analytical predictions. The results of measurements and the analyses in fig. 8 show good overall agreement. The results also demonstrate quantitatively the effect that material properties have on the effectiveness of the long pulse excitation method. For the high thermal conductivity aluminium alloy test piece very few of the defects produced images with measureable contrasts whilst the same size and depth defects produced strong contrasts in the low thermal conductivity CFRP and stainless steel test pieces. For example, in the aluminium alloy test piece the image of the 15 mm diameter 1 mm deep defect had a contrast of only 0.2 °C whilst for a similar defect in CFRP the contrast was found to be ~3 °C. This huge difference is due to the huge difference in the thermal response rates of the two materials, as explained in section 2. It shows, in general, that the long pulse excitation technique is unsuitable for the testing of high thermal conductivity materials such as aluminium and it also shows that it is very suitable for the testing of low thermal conductivity materials such as CFRP and stainless steel. This “general” rule can be made quantitative by reference to relationship between the effective efficiency of the long pulse method and peak contrast time shown in fig. 3. This figure shows that the substantial fall in effectiveness of the long pulse excitation method only occurs where peak contrast time is significantly less than 1 second. Flash excitation peak contrast time depends on both thermal properties and defect geometry: depth and diameter. Consequently, a very shallow defect in a low thermal conductivity material may have a peak contrast time that is much shorter than 1 second, making the long pulse excitation technique less suitable for its detection. Similarly, a very deep defect in a high thermal conductivity material may have peak contrast time approaching a second, making it more suitable for detection by the technique.

For all thermographic NDE techniques, defect detection sensitivity is linearly dependent on the excitation energy employed. Here, for the flash excitation technique defect image contrast is proportional to impulse heating  $J_0$  and for the long pulse excitation technique it is proportional to the product  $Wt_p$ . In practice, a high  $Wt_p$  can be achieved far more readily than a high  $J_0$ . In this work we have used shuttered quartz halogen lamps to provide long pulse heating because they produce the repeatable, well defined and reasonably uniform pattern of heating required for detailed quantitative

experimental work. However, long pulse heating of similar or substantially higher magnitude could have been achieved in a wide variety of ways. Options include the use of: hot air blowers; heating blankets; radiant heaters; induction heating or even a gas torch. In addition, there is the simple increasing of the heating time  $t_p$ . By contrast, for the flash excitation technique we are limited to the use of high pulse energy optical flash lamps. The excitation energy  $J_0$  is obtained from the absorption of a very high intensity flash of light emitted over a period of  $\sim 1$ - $2$  ms. The flash lamps available are produced for specialist photographic applications. Whilst the lamps are similar in size to the quartz halogen lamps, used for long pulse excitation, a bulky pulse power supply is necessary to drive them. The Hensel xenon flash lamps used were driven by a Hensel TRIA 600S generator whose dimensions are  $34.5 \times 19.5 \times 44$  cm and whose weight is 17 kg. The quartz halogen lamps were, of course, driven directly by mains electricity, and simply switched on and off as required. The heating of  $\sim 3 \text{ kJm}^{-2}$  achieved by the flash lamps was similar to what has been reported in a detailed calorimetric study [19] of the performance of these lamps. It is recognised that the setup indicated by figure 4 is very inefficient. There is a great deal of light spill from the lamps that results in much of the optical energy emitted failing to reach the test piece. The heating could be increased considerably by a carefully designed flash-hood that would contain and concentrate the light on the test piece and bring the flash lamp filaments closer to the test piece surface. For example, we found a heating of between 2.5 and 3  $\text{kJm}^{-2}$  for the commercial Thermoscope 1 [11] system which has a flash-hood and only a single 2 kJ flash lamp. This is a factor of three times more efficient than the basic setup, fig. 4, employed here where an electrical pulse energy of 6 kJ produces a similar heating. However, the design and construction of effective flash hoods requires considerable experience and expertise and the majority of workers, not using commercial systems, make use of off-the-shelf flash lamps in a similar way to what we have done here. The ultimate performance of their systems depend on the heating produced by the flash lamps and we have found that this is much lower than can be readily provided by a pair of 1 kW quartz halogen lamps using the long pulse excitation technique. It is also notable that the flash excitation equipment used here cost  $\sim 100$  times more than the equipment used for long pulse excitation.

The step heating method, mentioned in the Introduction, has a number of disadvantages. As thermal imaging is performed during heating, the lamp emissions have to be passed through suitable filters, typically sheets of Plexiglass (poly(methyl methacrylate) or PMMA), to absorb infrared radiation that would otherwise saturate the IR camera. This radiation, however, is a major component of quartz halogen lamp output and a major contributor to the heating capability of these lamps. Consequently, the removal of this radiation reduces considerably the heating flux  $W$  achieved at an exposed test piece surface. In addition, the effective excitation energy density  $Wt$  varies continually with time during step heating. By contrast, for long pulse heating no filters are necessary and the full heating potential of the lamps is used as thermal images are only collected after the completion of heating. The use of shutters ensures that clean purely thermal images are collected, uncontaminated by residual lamp emission, which maximises defect image thermal contrast. Shutters are 100% effective in this whilst filters are sure to be less effective leaving a background of scattered lamp radiation that will reduce image contrast.

In this work, we have only considered the basic thermal contrast produced by a defect. The images presented are of raw data and the contrasts measured and presented for comparison with theory are of this same raw data. There are a number of image processing techniques [20-22] that have been shown to enhance defect images. These techniques make use of the image data in all of the frames collected in the thermal transient following excitation rather than just the frame exhibiting peak contrast. There is a consequent enhancement in the quality of the defect image and a reduction in the effective noise. For one of these, Thermographic Signal Reconstruction (TSR) [20], there has been [15] a quantitative comparison of the performances of step heating thermography with flash thermography. TSR involves fitting a polynomial function to the temporal dependence of each pixel of the thermal images collected during a test. From these functions, first and second time derivative images may be generated and these are often distinctly clearer than raw data images. It was found [15] overall that flash excitation images obtained in this way were superior to those obtained using step heating. However, there is no indication of the relative values of  $J_0$  and  $Wt$  so it is not possible to

be sure that there is an inherent superiority of flash excitation over step heating. A comparison of flash and long pulse images processed using TSR would be a useful future work.

## 6. Conclusions

An analysis of the defect imaging process and the comprehensive experimental investigation presented here show there to be a strong case for considering the use of long pulse excitation as an alternative to traditional flash excitation in thermographic NDE. In general, long pulse excitation is very effective for the detection of defects in low thermal conductivity, low thermal response rate materials such as plastics and resin based composites (CFRP, GFRP). An analytical method for estimating the thermal image contrast of specified defects in any material has been developed and shown to be in good agreement with experimental measurements. An unexpected outcome of the experimental programme was the strong performance of the long pulse technique in detecting defects in the intermediate conductivity material stainless steel.

It has been noted that the performance of flash excitation thermographic NDE is limited by the magnitude of the impulse heating,  $J_0$ , produced by available flash lamps. For long pulse heating, however, there are a wide variety of heat sources that can be used and the heating produced by these,  $Wt_p$ , can readily exceed by many times typical values of  $J_0$ . In addition, the heat sources that may be used for long pulse heating are widely available and are very much less expensive than the specialist high energy flash lamp systems necessary for flash excitation thermographic NDE. It is therefore suggested that the traditional flash excitation technique should only be employed where it is essential, ie for the inspection of high thermal conductivity, high thermal response rate materials, for which the long pulse technique has been shown to be ineffective. For other materials, it is likely that the long pulse excitation technique will substantially out-perform the flash excitation technique because of the ease of producing long pulse heating of a magnitude that substantially exceeds typical values achieved by impulse heating. The alternative selection of long pulse excitation for a particular application is incorporated in our thermographic NDE expert system: The Thermographic NDE Advisory and Guidance System [23].

## **Acknowledgements**

This work was part of the Core Research Programme of the UK Research Centre in NDE (RCNDE) supported by the UK Engineering and Physical Science Research Council (EPSRC).

## **References**

- [1] Milne J M and Reynolds W N. The non-destructive evaluation of composites and other materials by pulsed video thermography. Proc. Soc. Photo- Optical Instrumentation Eng. 1985, **520**, 119-122.
- [2] Reynolds W N and Wells G M. Video-compatible thermography. Brit. J. NDT. 1984, **26**, 40-44.
- [3] Green D R. Emissivity-independent infrared thermal testing method. Mater. Eval., 1965;23(2):79-85.
- [4] Carlomagno GM and Berardi PG. Unsteady thermophototopography in non-destructive testing. Proc. 3<sup>rd</sup> Biannual Exchange. 1976, 33-39.
- [5] Vavilov V P and Burleigh D D. Review of pulsed thermal NDT: Physical principles, theory and data processing. NDT&E International, 2015, 73, 28-52.
- [6] Busse G, Wu D, Karpen W. Thermal wave imaging with phase sensitive modulated thermography. J. Appl. Phys., 1992, **71** , 3962-3965.
- [7] Tuli S and Mulaveesala R. Defect detection by pulse compression in frequency modulated thermal wave imaging. J. Quantitative Infrared Thermography. 2012, 2, 41-54.
- [8] Valivov V P. Infrared NDT of bonded structures. Brit. J. NDT. 1981, 175-183.
- [9] Vavilov V P and Taylor R. Theoretical and practical aspects of the thermal non-destructive testing of bonded structures. Research Techniques in Nondestructive testing, Vol. 5, Academic Press, London, 1982, 239-279.

- [10] Almond D P, Delpech P, Peng Wang and Behesty M. Quantitative determination of impact damage and other defects in carbon fiber composites by transient thermography. Proc. SPIE 1996, **2944**, 256-264.
- [11] Thermal Wave Imaging, Inc. Ferndale MI, USA.
- [12] C-Checkir, Automation Technology GmbH, Bad Oldesloe, Germany.
- [13] Osiander R and Spicer J W M. Time resolved radiometry with step-heating – A review. Rev. Gen. de Thermique. 1998, **37**, 680-692.
- [14] Badghaish A A and Fleming D C. Non-destructive inspection of composites using step heating thermography. J. Composite Materials. 2008, **42**, 1337-1357.
- [15] Roche J –M and Balageas D. Common tools for quantitative pulse and step-heating thermography-Parts I and II. QIRT 2014 Conference, Bordeaux, France, 1-28.
- [16] Almond D P and Pickering S G. An analytical study of the pulsed thermography defect detection limit. J. Appl. Phys. 2012, **111**, 093510.
- [17] Lau S K, Almond D P and Patel P M. Transient thermal wave techniques for the evaluation of surface coatings. J. Phys, D: Appl. Phys. 1991, **24**, 428-436.
- [18] Hensel Studiotecnic, Würzburg Germany.
- [19] Krankenhagen, R and Maierhofer Ch. Determination of the spatial energy distribution generated by means of a flash lamp. Proc. 11<sup>th</sup> Int. Conf. on Quantitative Infrared Thermography (QIRT 2012). 2012, 1-10.
- [20] Shepard S M, Lhota J R, Rubadeaux B A, Wang D and Ahmed T. Reconstruction and enhancement of active thermographic image sequences. Optical Engineering, 2003, **42**, 1337-1342.
- [21] Maldague X and Marinetti S. Pulse phase infrared thermography. J. Appl. Phys. 1996, **79**, 2694-2698.



[22] Rajic N. Principal component thermography for flaw contrast enhancement and flaw depth characterization in composite structures. *Comp. Structures*, 2002, **58**, 521-528.

[23] Almond D P, Angioni S L and Pickering S G. Thermographic NDE advisory and guidance system. *NDT&E International*, 2016, **83**, 134-142.

### **Figure captions**

**Figure 1.** Thermal contrast vs. elapsed time for a 5mm diameter defect 1mm beneath the surface of a mild steel sample calculated by finite difference modelling (FD) and the analytical model, eqn.1, (Analytic 2). Pulse intensity  $10 \text{ kJ m}^{-2}$ .

**Figure 2.** Finite difference simulation of long pulse thermal contrast vs. time for 5mm diameter 1mm deep defects in materials indicated. 5 second heating of  $1\text{kWm}^{-2}$ .

**Figure 3.** Ratio of long pulse to flash peak contrast shown as a function of flash contrast peak time.

**Figure 4.** Schematic diagram of the long pulse excitation thermographic NDE system.

**Figure 5.** Long pulse and flash excitation images of the aluminium alloy, mild steel and stainless steel test pieces.

**Figure 6.** Long pulse and flash excitation images of the CFRP test piece obtained at 5, 10, 15 and 20 seconds after heating.

**Figure 7.** (a) Schematic diagram showing the locations of the four boxes of pixels around a defect image used to estimate background heating and the smaller box of pixels within image used to estimate image contrast. (b) Schematic timing diagram for a typical pixel showing the effect of heating and subsequent cooling on the recorded digital signal.

**Figure 8,** Measurements of the contrasts of the long pulse excitation images, shown in figures 5 and 6, of the defects compared with contrasts predicted by the analytical method outlined in section 2.

